Glaucoma Detection and Classification Based on Image Processing and Artificial Neural Networks

Kamel H. Rahouma, Marwa M. Mohamed and Nagwa S. Abdel Hameed

Faculty of Engineering, Minia University, Minia, Egypt

kamel_rahouma@yahoo.com, eng.marwa.medhat@gmail.com, nagwa_minia@yahoo.com

Abstract

Glaucoma is considered the second cause of blindness worldwide. It damages the optic nerve causing irreversible blindness if it doesn't be early detected. This paper aims to detect and classify Glaucoma. It adopts the Grey Level Co-occurrence Matrix (GLCM) and Gray-Level Run Length Matrix (GLRLM) methods to extract 29 statistical texture features. Then, the artificial neural network (ANN) is trained with the back propagation technique for classification. MATLAB is used for image processing and computation. Accuracy is found to be 99% which is one of the highest levels compared with the existing research.

Keywords: *Glaucoma, Feature Extraction, Glaucoma Detection, Glaucoma Classification, Image Processing, Artificial Neural Networks.*

1. Introduction

According to the World Health Organization (WHO) reports, there are 285 million people having visual impairment in the whole world. Thirty nine millions of them are blind, and 246 have low vision. Glaucoma is considered the second cause of blindness worldwide. It damages the optic nerve causing irreversible blindness if it doesn't be early detected [1]. Increasing intraocular pressure (IOP) is the major cause of Glaucoma in addition to other risk factors as old age, ethnic background, family history of Glaucoma and high myopia. However, in some cases Glaucoma may occur at normal IOP due to poor blood flow regulation to the optic nerve [2]. This disease is painless and doesn't have noticeable symptoms. Since most cases of patients don't realize that they have this disease till reaching a late stage and the correct diagnosis require ophthalmologists who have sufficient experience as well as the medical examinations such as Ocular coherence tomography (OCT) and Heidelberg retinal tomography (HRT) which have high costs, and they require special equipment and consume time [3, 4]. So, the need for a computer aided diagnosis system is urgent.

Here we introduce a system relying on image processing techniques which allow us to extract features from eye fundus images that are used by ophthalmologists in order to detect and diagnose Glaucoma where its cost isn't high. This system will be helpful in early Glaucoma detection that provides an opportunity for ophthalmologists to intervene and slow down its progression by any suitable treatment.

This paper includes 6 sections. Section (1) is an introduction and section (2) introduces a literature review. Section (3) explains the methodology of this research and section (4) gives the results. Section (5) discusses the results and compares them with the results obtained from previous research while section (6) highlights some conclusions. A list of the used references is given at the end of the paper.

2. A Literature review

A great effort has been made, and numerous studies have been presented by many researchers. The RGB fundus images are converted to grayscale then Gaussian filter and adaptive histogram equalization are used for noise removal and contrast enhancement. Then, sixteen features are extracted by using Grey Level Co-occurrence Matrix (GLCM) and Gray-Level Run Length Matrix (GLRLM). Finally, the Support Vector Machine (SVM) is trained by K-fold cross-validation. The SVM classifies the images to Glaucoma or normal eye fundus [3].

The optic disk and optic cup are the most important area of the RGB fundus images. So, an area around the optic disk is extracted which is called region of interest (ROI) then the red channel and the green channel were used to detect the optic disk and optic cup respectively. Otsu segmentation is used to segment both optic disk and cup. After segmentation the features Cup to disk ratio (CDR) and rim to disk ratio (RDR) are obtained, and threshold values are used to classify images [4].

Suspected Glaucoma is detected by depending on appearance or disappearance of hemorrhages on the optic disk or near it that is considered as a sign of damage [2]. Various fundus images from different databases are used and cropped to get the ROI and segmented by using Region Growing Method and Watershed Transform. Then, the outputs of the two methods are combined to get one segmented optic disk and cup followed by CDR and neuroretinal rim (NRR) calculation to classify the images [5].

The RGB fundus images are converted to red channel to detect the optic disk and segment it. Then, texture features are extracted by using GLCM and entropy in three different color modes and the classification is made by four methods [6]. A system based on hybrid feature extraction is introduced where the colored images are converted to greyscale, enhanced contrast with histogram equalization and radon transform converts the 2D images to 1D signal [7]. Multiple features such as phase entropy, bi-spectrum entropy using Higher Order Spectra (HOS), triple feature using Trace Transform (TT), and average energy of wavelet coefficients are extracted and then, the SVM classifies the images.

Another technique depends upon bit-plane slicing (BPS) and local binary patterns (LBP) where the three channels of the images are separated and split into bit planes and LBP features are extracted from every bit plane for all the channels. Subsequently, the features are supplied to three SVMs and the outputs are combined for classification [8].

3. The Methodology

We introduce a system for Glaucoma detection from fundus images based on texture features. The block diagram in fig. 1 demonstrates our methodology and in the following subsections, we explain every part of this diagram.

3.1. RGB Fundus Images

We use the public database Retinal Image for Optic Nerve Evaluation (RIM-ONE) which maintains a gold standard accuracy. It's the result of effective cooperation of three Spanish hospitals: Hospital Universitario de Canarias, Hospital Clínico San Carlos and Hospital Universitario Miguel Servet. They aim to make a reference point for designing segmentation algorithms of optic nerve head and for developing computer aided diagnosis systems of Glaucoma. It consists of three releases containing retinal fundus images obtained by ophthalmologists' experts. We use We use 614 images from RIM-ONE Release 3 and

Rim-ONE Release 2 (340 are normal and 274 are Glaucoma). The images were captured by Nidek AFC-210 background camera with a 21.1-megapixel Canon EOS 5D Mark II body [9, 10].

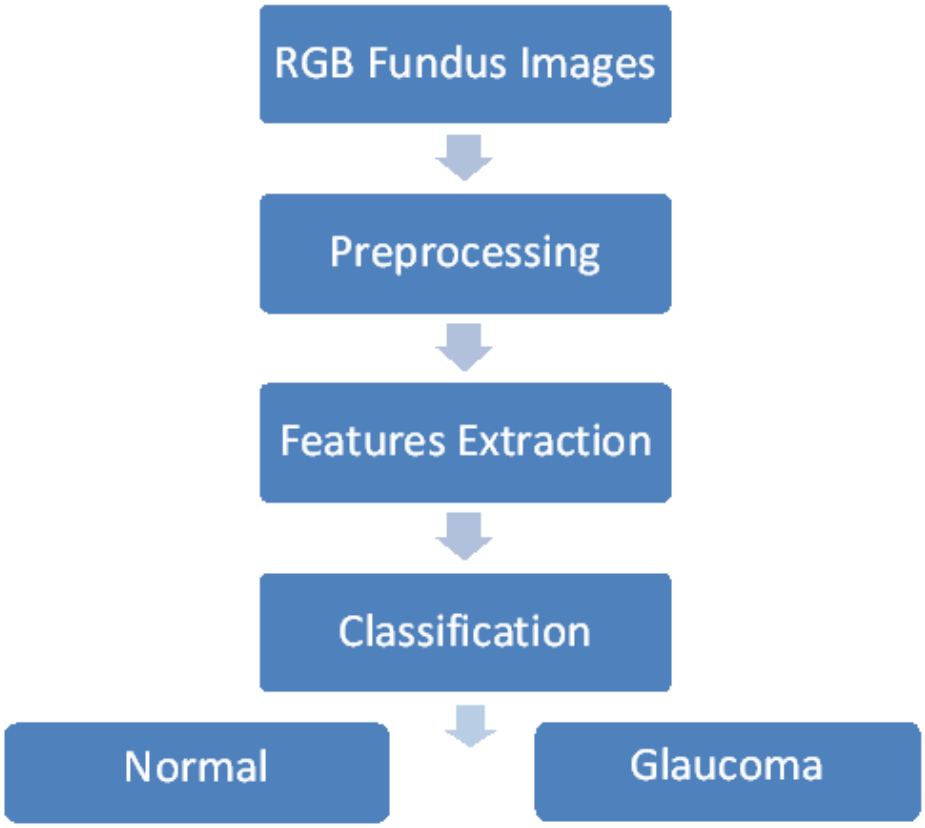

Figure (1): Block diagram of the Glaucoma detection system

3.2. Preprocessing

The images didn't need much preprocessing, we only converted them from RGB to greyscale and trimmed to focus on the ROI which is the optic disk.

3.3. Features Extraction

We adopt Gray-Level Co-occurrence Matrix GLCM and GLRLM methods to extract 29 statistical texture features. This is explained in the following subsections.

3.3.1. Gray-Level Co-occurrence Matrix (GLCM)

The GLCM is considered a method for calculating the second order texture features. Second order means taking into account the relationship between two pixels. GLCM demonstrates the spatial relationship between each intensity tone by considering changes between gray levels i and j at a certain distance d and at a certain angle θ. Formally, the

G × G Gray-Level Co-occurrence Matrix P for a displacement vector d = (dx, dy) is defined as follows where the entry (i, j) of P is the number of occurrences of the pair of gray levels i and j which are at distance d apart.

$P(i, j) = \{((r, s), (t, v)): I(r, s) = i, I(t, v) = j \mid (r, s), (t, v) \in N \times N, (t, v) = (r + dx, s + dy)\}$ [3].

After creating GLCM of a preprocessed input image, we set d = 1 and θ = 0° for extracting the features below:

Grey level Co-occurrence Matrix (p (i, j)):

$p_x(i) = \sum_{j=1}^{N_g} p(i,j)$,

$p_y(i) = \sum_{j=1}^{N_g} p(i,j)$,

$p_{x+y}(k) = \sum_{i}^{N_g} \sum_{j}^{N_g} p(i,j) \;\; k = 2,3,\dots 2N_g$,

$p_{x-y}(k) = \sum_{i}^{N_g} \sum_{j}^{N_g} p(i,j) \;\; k = 0,1,\dots N_g - 1$,

$H_{xy1} = -\sum_i \sum_j p(i,j) \log\{p_x(i)p_y(j)\}$;

$H_{xy2} = -\sum_i \sum_j p(i,j) \log\{p_x(i)p_y(j) \log\{p_x(i)p_y(j)\}$,

Where μ_x, μ_y, σ_x, σ_y, H_x, H_y are the means, standard deviations, and entropies of p_x and p_y. Table (1) gives the features of the GLCM [11].

Table (1) GLCM's Features

Number	Feature	Equation
1.	Contrast	$\sum_i \sum_j \lvert i-j\rvert^2 p(i,j)$
2.	Correlation1	$\sum_i \sum_j \frac{(i-\mu_x)(j-\mu_y)p(i,j)}{\sigma_x \sigma_y}$
3.	Correlation2	$\sum_i \sum_j \frac{(i,j)p(i,j) - \mu_x \mu_y}{\sigma_x \sigma_y}$
4.	Dissimilarity	$\sum_i \sum_j \lvert i-j\rvert p(i,j)$
5.	Energy	$\sum_i \sum_j p(i,j)^2$
6.	Entropy	$-\sum_i \sum_j p(i,j) \log_2(p(i,j))$
7.	Autocorrelation	$\sum_i \sum_j (i,j)p(i,j)$
8.	Homogeneity1	$\sum_i \sum_j \frac{p(i,j)}{1+\lvert i-j\rvert}$
9.	Homogeneity2	$\sum_i \sum_j \frac{p(i,j)}{1+(i-j)^2}$
10.	Sum average	$\sum_{i=2}^{2N_s} i.p_{x+y}(i)$
11.	Sum entropy	$-\sum_{i=2}^{2N_s} p_{x+y}(i) \log_2(p_{x+y}(i))$
12.	Sum variance	$\sum_{i=2}^{2N_s} (i - sum\ entropy)^2 . p_{x+y}(i)$
13.	Difference variance	$\sum_{i=0}^{N_s-1} i^2 . p_{x-y}(i)$

Follow Table (1) GLCM's Features

Number	Feature	Equation
14.	Difference entropy	$\sum_{i=0}^{N_s-1} p_{x-y}(i)\log_2(p_{x-y}(i))$
15.	Information measure of correlation1	$\frac{Entropy - H_{XY1}}{\max(H_X H_Y}$
16.	Information measure of correlation2	$\sqrt{(1-\exp(-2(H_{XY2}-Entropy)))}$
17.	Cluster Prominence	$\sum_i \sum_j (i+j-\mu_x-\mu_y)^4 p(i,j)$
18.	Cluster Shade	$\sum_i \sum_j (i+j-\mu_x-\mu_y)^4 p(i,j)$
19.	Maximum Probability	p (i j)
20.	Sum of Squares	$\sum_i \sum_j (i-\mu)^2 p(i,j)$
21.	Inverse Difference Normalized	$\sum_i \sum_j \frac{p(i,j)}{1+(\lvert i-j\rvert/N_g)}$
22.	Inverse Difference Moment Normalized	$\sum_i \sum_j \frac{p(i,j)}{1+((i-j)/N_g)^2}$

3.3.2. Grey Level Run Length Matrix (GLRLM)

The GLRLM is also a technique for computing the second order texture features. The run length matrix P_θ (i, j) is computed where every cell in the matrix comprises a bit of elements where gray level i shows up j times towards θ direction. Run length is defined as j. The output matrix describes the gray-level runs by the gray tone, length, and the direction of the run [3]. GLRLM's texture features are given in table (2) [12, 13].

3.4. Classification

We use the artificial neural network (ANN) trained with back propagation technique. It is a supervised classifier consists of an input layer which contains the elements of the matrix of the extracted features, output layer which represents the two classes and one or more intermediate layers known as hidden layers that involve countless neurons [14, 15]. Back propagation is the most broadly utilized algorithm in neural networks. It uses gradient descent to minify the squared error between the calculated output value and the coveted output value [16]. Table (3) represents the principal equations [17].

Table (2) GLRLM's Features

Number	Feature	Equation
1	Long run emphasis (LRE)	$\frac{\sum_i \sum_j j^2 P_{\theta(i,j)}}{\sum_i \sum_j P_{\theta(i,j)}}$
2	Short run emphasis (SRE)	$\frac{\sum_i \sum_j \frac{P_{\theta(i,j)}}{j^2}}{\sum_i \sum_j P_{\theta(i,j)}}$

3	Gray-level non-uniformity (GLNU)	$\frac{\sum_i \sum_j \{P_{\theta(i,j)}\}^2}{\sum_i \sum_j P_{\theta(i,j)}}$
4	Run length nonuniformity (RLNU)	$\frac{\sum_i \sum_j \{P_{\theta(i,j)}\}^2}{\sum_i \sum_j P_{\theta(i,j)}}$
5	Run percentage (RP)	$\frac{\sum_i \sum_j P_{\theta(i,j)}}{A}$ A is the area of interest the image
6	Low gray level run emphasis (LGRE)	$\sum_{i=1}^{\hat{M}} \sum_{j=1}^{\hat{N}} \frac{P(i,j)/s}{i^2}$
7	High gray level run emphasis (HGRE).	$\sum_{i=1}^{\hat{M}} \sum_{j=1}^{\hat{N}} \frac{i^2 P(i,j)}{s}$

Table (3) Back-propagation Equations of the system

Number	Name	Equation
1	The activation vector (a^l)	$a^l = \sigma(w^l a^{l-1} + b^l)$ Where w^l 's weight matrix, b^l 's bias vector.
2	Cost function (C)	$c = \frac{1}{2n} \sum_x \|\|y(x) - a^L(x)\|\|^2$ y(x) is the desirable output, L is the number of layers, $a^L = a^L(x)$ vector of activations output.
3	Sigmoid function (activation function)	$\sigma(x) = \frac{1}{1+e^{-x}}$
4	Weighted input to neurons (z^l)	$z^l = w^l a^{l-1} + b^l$
5	The error vector	$\delta^L = \nabla_a C \odot \sigma'(z^L)$
6	The error δ^l in terms of the error in the next layer, δ^{l+1}	$\delta^l = ((w^{l+1})^T \delta^{l+1}) \odot \sigma'(z^l)$ $(w^{l+1})^T$is the transpose of the weight matrix w^{l+1} for the layer $l+1^{th}$
7	Change cost according to change bias	$\frac{\partial C}{\partial b_j^l} = \delta_j^l$
8	Change cost according to change weight	$\frac{\partial C}{\partial w_{jk}^l} = a_k^{l-1} \delta_j^l$

3.5 The System Algorithm

1. Read input images.
2. Convert them from RGB to Gray.
3. Extract ROI automatically by bounding box.
4. Apply equations in table (1).
5. Apply equations in table (2).
6. Construct the network.
7. Provide the network with the input and decide the target.
8. Apply equations from 3 to 8 in table (3).
9. Detect Glaucoma.

3.6 The System Flow chart

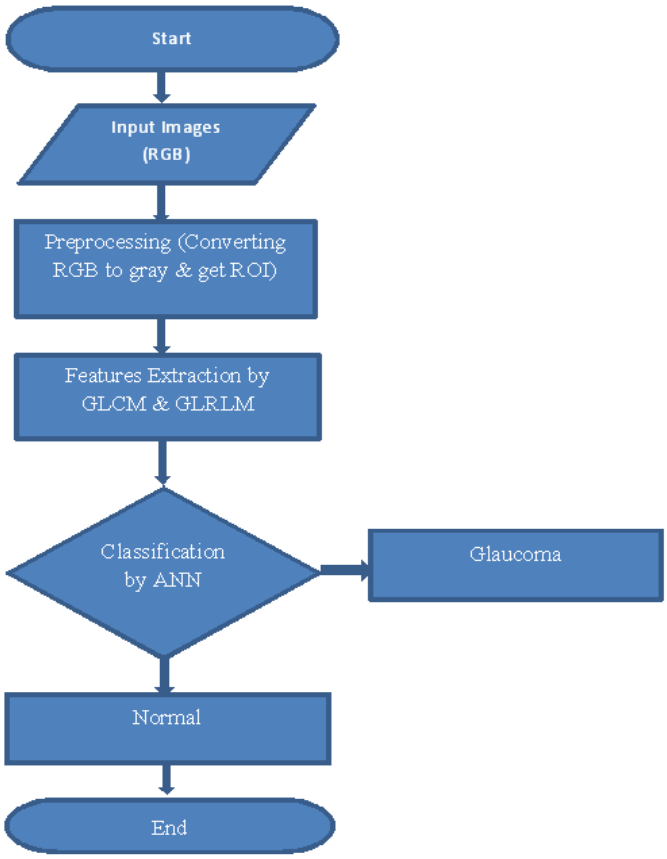

Figure (2): The system flow chart

4. Results

We developed our system in Matlab version 8.2 (R2013b) and on laptop with core i3 processor, 2G RAM and 32-bit operating system.

In our study we tried three different techniques in the feature extraction stage. In the first one, we extracted the GLCM's features then fed them to ANN classifier. The accuracy was found to be 70.4% as shown in fig (3). Second, we fed the GLRLM's features to the same classifier and the accuracy was found to be 76.7% as shown in fig (4). Finally, we combined the features of the both previous techniques and the accuracy was found to be 89.3% as presented in fig (5). Our results are demonstrated in table (4):

Table (4): Results of our system

Number	Method	Sensitivity	Specificity	Accuracy
1	GLCM	70%	70%	70.3%
2	GLRLM	88%	80%	76.7%
3	GLCM & GLRLM	98%	90%	89.3%

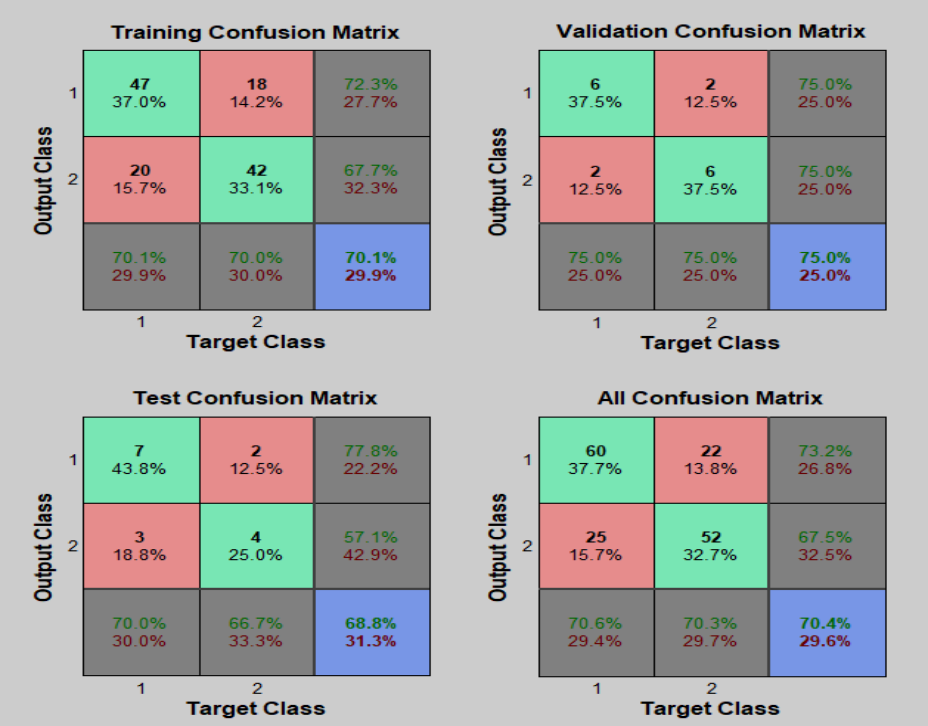

Figure (3) Convolution matrix of ANN when using GLCM's features

5. Discussion and comparison of the results

As demonstrated in table (4), we got the highest accuracy, sensitivity and specificity which are 89.3%, 98% and 90% respectively when we combined the features that we extracted by using GLCM and GLRLM. When we separately used GLCM and GLRLM for features extraction, GLRLM provided better accuracy, sensitivity and specificity than using GLCM.

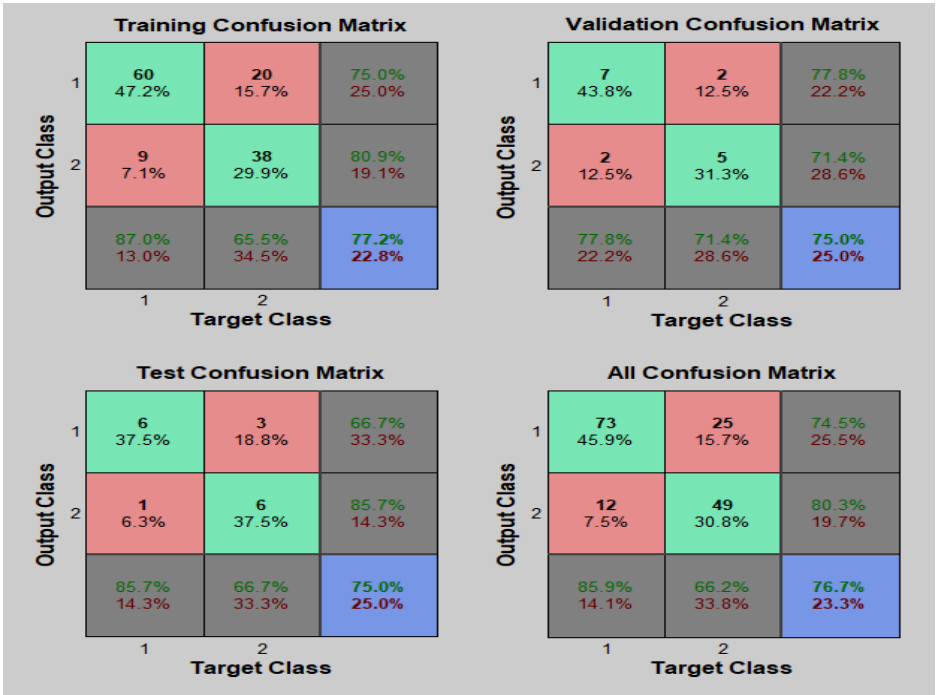

Figure (4) Convolution matrix of ANN when using GLRLM's features

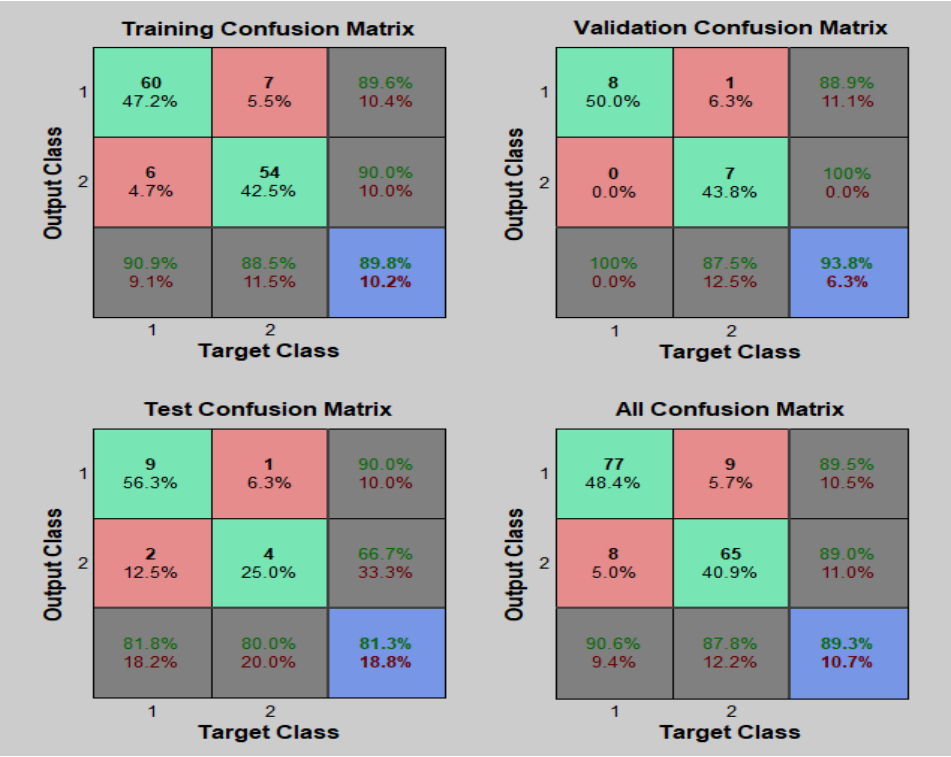

Figure (5) Convolution matrix of ANN when combining GLCM & GLRLM features

Our system is based on texture features that are extracted by two different methods. The advantages of our methodology are:

1) It doesn't require segmentation as it plays out a statistical data extraction technique on images patterns.
2) It has a high robustness versus inter and intra image variance if it is designed carefully [18].
3) Moreover, it doesn't rely on specific threshold values for classification that aren't standardized.

Some of the systems are dependent on morphological features such as CDR, RDR and inferior superior nasal temporal (ISNT) method. This conduce imprecise results due to inexact segmentation of optic disk and optic cup because of appearance of bright lesions. In addition, the detection of optic cup area is one of the difficult undertakings as the color intensity of the cup doesn't much vary from optic disk and the blood vessels intervene with optic disk boundary and cover part of them [19]. Also, these methods adopted classification based on threshold values of their features which differ from study to another. For example, some of them set 0.3 as CDR threshold value. Others set it by 0.5. Furthermore, some patients are infected with Glaucoma although their CDR ratios are still in the acceptable range. So, these features aren't reliable [20].

Table (5): Comparison between Automated Glaucoma detection techniques mentioned in this research

Reference	Features Extraction Method	Classifier	Database	Accuracy
[3](Dey & Dey,2018)	GLCM & GLRLM	SVM	100 images (50 normal & 50 Glaucoma) from Susrut Eye Foundation and Research Centre, Kolkata.	97%
[4](Indexed et al., 2017).	CDR & RDR Structural features	Thresholding based on CDR & RDR values	STARE Public database	Not mentioned
[2](Sengar et al., 2017).	Hemorrhages detection	According to Hemorrhages appearance	140 images (100 normal & 40 suspected Glaucoma) from local hospital	93.57%
[5](Das et al., 2016).	CDR and ISNT rule	Depending on CDR & NRR values	244 images (163 normal & 81 Glaucomatous) from Four public databases (HRF, Messidor, DRIONS-DB, DIARETDB1) and a domestic eye hospital (Sri Sankaradeva Netralaya).	93.85 %
[6](Claro et al., 2016).	GLCM and entropy	MultiLayer Perceptron (MLP), Radial Basis Function (RBF), Random Committee and Random Forest	329 images from three public databases (RIM-ONE, DRISTHIGS and DRIONS-DB)	93%
[7](KRISHNAN & FAUST, 2012).	HOS, TT, DWT and Energy features	SVM	60 images (30 normal and 30 Glaucomatous) from the Kasturba Medical College, Manipal, India.	91.67%
[8](Maheshwari et al., 2019)	Local binary pattern (LBP) based features.	SVM & decision level based fusion technique	1426 images (589 normal and 837 Glaucomatous) from Kasturba Medical College, Manipal, India	99.30%
Our system results	GLCM and GLRLM	ANN	614 images (340 are normal and 274 are Glaucomatous) from Rim-One public database	99%

Table (5) summarizes and compares between our system results and the results of the researches which we previously introduced in the literature review section. In this table we can highlight the following points:

1) Authors in [3] used 16 features, 5 for GLCM and 11 for GLRLM. For the classification they used SVM with four different kernels: Linear kernel, Polynomial Kernel, RBF (radial basis function) Kernel and Sigmoid Kernel. They tried each one of them separately and compared between their accuracies. Every one of them has its own parameters. So, the proper parameters' selection is effective in achieving a total high accuracy of 97%.
2) Authors in [2] based the detection of Glaucoma on appearance and disappearance of hemorrhages. They considered this internal bleeding near the optic disk as a sign of Glaucoma. They use the green channel of the image to detect hemorrhages then adaptive thresholding is used to segment the image and remove blood vessels. Finally, geometrical features such as major and minor axis length and the diameter of detected hemorrhages are used to decide the right hemorrhages. This resulted in an accuracy of 93.57%.
3) Authors in [5] used two different methods for the segmentation of the optic disk and the optic cup. Region growing method and Watershed transform are combined to get higher reliability. After that, CDR and ISNT are extracted to classify images. This resulted in an accuracy of 93.85%.
4) Authors in [6] extracted the red channel and then the images are segmented to detect the optic disk. GLCM and Entropy are used to extract the features. At the end four different classifiers are used to classify the images. This resulted in an accuracy of 93%.
5) Authors in [7] converted the 2D image into 1D signal by radon transform. Four features are extracted by using different techniques and SVM with three different kernels: Linear, Polynomial degree 2, Polynomial degree 3 and RBF are used for classification. The highest accuracy is achieved by using the SVM with Polynomial degree 2 kernel. This resulted in an accuracy of 91.67%.
6) Authors in [8] used a massive dataset. The image's channels are separated and divided into several bit planes. The LPB features are extracted and fed to three SVMs. Outputs of the SVMs are merged at decision level to classify images. This resulted in an accuracy of 99.3%.
7) In our system, we use 29 features: 22 for GLCM and 7 for GLRLM. ANN with 10 hidden layers is used for classification. 80% of the dataset are used for training and 20% for testing. At the beginning we only use 159 images as input images (85 normal images and 74 Glaucoma images). The accuracy, sensitivity and Specificity were 89.3%, 98% and 90% respectively. Then we enlarge our dataset to become containing 614 images (340 normal images and 274 Glaucoma images). The accuracy, sensitivity and Specificity raised to: 99%, 100% and 100% respectively.

6. Conclusions

This paper aimed to detect and classify the Glaucoma. Image processing is applied by employing the Grey Level Co-occurrence Matrix (GLCM) and Gray-Level Run Length Matrix (GLRLM) methods to extract 29 statistical texture features. These features are classified using back propagation of artificial neural networks (ANN). Ten hidden layers between the input and output layers are utilized. The number of images affects the resulted accuracy of the detection and classification. When 159 images are used (85 normal images and 74 Glaucoma images), the accuracy is found to be 89.3%. When the number of images is increased to 614 (340 normal images and 274 Glaucoma images), the accuracy is increased to 99% which is one of the highest accuracies compared with the previous research results.

References

[1]. Adjei, P. E. (2016). A new image processing algorithm for computer aided prediction of Glaucoma in Ghana, M.Sc. thesis, Department of Computer Engineering, College of Engineering, Kwame Nkrumah University of Science and Technology, Ghana.

[2]. Sengar, N., Dutta, M. K., Burget, R., & Ranjoha, M. (2017). Automated detection of suspected Glaucoma in digital fundus images. 2017 40th International Conference on Telecommunications and Signal Processing, TSP 2017, 2017-January, 749–752. https://doi.org/10.1109/TSP.2017.8076088

[3]. Dey, A., & Dey, K. N. (2018). Industry Interactive Innovations in Science, Engineering and Technology. 11. https://doi.org/10.1007/978-981-10-3953-9

[4]. Indexed, S., Devi, M. S., Sruthi, A. N., & Vinodhini, S. (2017). Automatic Detection of Glaucoma Through Channel Extraction Adaptive Threshold Method. 8(11), 69–77.

[5]. Das, P., Nirmala, S. R., & Medhi, J. P. (2016). Diagnosis of Glaucoma using CDR and NRR area in retina images. Network Modeling Analysis in Health Informatics and Bioinformatics, 5(1). https://doi.org/10.1007/s13721-015-0110-5

[6]. Claro, M. de L., Santos, L. de M., Lima e Silva, W., de Araújo, F. H. D., de Moura, N. H., & Santana, A. M. (2016). Automatic Glaucoma Detection Based on Optic Disc Segmentation and Texture Feature Extraction. CLEI Electronic Journal, 19(2), 4:1-4:10. https://doi.org/10.19153/cleiej.19.2.4

[7]. KRISHNAN, M. M. R., & FAUST, O. (2012). Automated Glaucoma Detection Using Hybrid Feature Extraction in Retinal Fundus Images. Journal of Mechanics in Medicine and Biology, 13(01), 1350011. https://doi.org/10.1142/s0219519413500115

[8]. Maheshwari, S., Kanhangad, V., Pachori, R. B., Bhandary, S. V., & Acharya, U. R. (2019). Automated Glaucoma diagnosis using bit-plane slicing and local binary pattern techniques. Computers in Biology and Medicine, 105, 72–80. https://doi.org/10.1016/j.compbiomed.2018.11.028

[9]. Gómez-Valverde, J. J., Antón, A., Fatti, G., Liefers, B., Herranz, A., Santos, A., … Ledesma-Carbayo, M. J. (2019). Automatic Glaucoma classification using color fundus images based on convolutional neural networks and transfer learning. Biomedical Optics Express, 10(2), 892. https://doi.org/10.1364/boe.10.000892

[10]. Medical Image Analysis Group(MIAG). (n.d.). Retrieved from http://medimrg.webs.ull.es/research/retinal-imaging/rim-one/

[11]. Mousa, D., Zayed, N., & Fakhr, M. (2017). Significant Features To Detect Pulmonary Nodules From Ct Lung Images. Biomedical Engineering: Applications, Basis and Communications, 29(06), 1750045. https://doi.org/10.4015/s1016237217500454

[12]. M.Galloway, M. (1975). Texture analysis using gray level run lengths. Computer Graphics and Image Processing, 172–179.

[13]. Park, B. E., Jang, W. S., & Yoo, S. K. (2016). Texture analysis of supraspinatus ultrasound image for computer aided diagnostic system. *Healthcare Informatics Research*, *22*(4), 299–304. https://doi.org/10.4258/hir.2016.22.4.299

[14]. Hagiwara, Y., Koh, J. E. W., Tan, J. H., Bhandary, S. V., Laude, A., Ciaccio, E. J., … Acharya, U. R. (2018). Computer-aided diagnosis of Glaucoma using fundus images: A review. Computer Methods and Programs in Biomedicine, 165, 1–12. https://doi.org/10.1016/j.cmpb.2018.07.012

[15]. T.R.Kausu, Varun P.Gopi, Khan A.Wahid, W. and S. I. N. (2018). Combination of clinical and multiresolution features for Glaucoma detection and its classification using fundus images. Biocybernetics and Biomedical Engineering, 329–341.

[16]. Soltani, A., Badaoui, A., Battikh, T., & Jabri, I. (2018). A Novel System for Glaucoma Diagnosis Using Artificial Neural Network Classification. 2018 5th International Conference on Control, Decision and Information Technologies, CoDIT 2018, 1128–1133. https://doi.org/10.1109/CoDIT.2018.8394940

[17]. A.Nielsen, M. (2015). How the back propagation algorithm works (chapter 2). In Neural Networks and Deep Learning. Retrieved from http://neuralnetworksanddeeplearning.com/chap2.html

[18]. Mohammad, S., & Morris, D. T. (2015). Texture analysis for Glaucoma classification. 2015 International Conference on BioSignal Analysis, Processing and Systems, ICBAPS 2015, 1, 98–103. https://doi.org/10.1109/ICBAPS.2015.7292226

[19]. Salam, A. A., Khalil, T., Akram, M. U., Jameel, A., & Basit, I. (2016). Automated detection of Glaucoma using structural and non structural features. SpringerPlus, 5(1). https://doi.org/10.1186/s40064-016-3175-4

[20]. Jost B Jonas, Tin Aung, Rupert R Bourne, Alain M Bron, Robert Ritch, S. P.-J. (2017). Glaucoma. The Lancet, 2183–2193.